Journal of Environmental Chemical Engineering 12 (2024) 113014

Contents lists available at ScienceDirect

Journal of Environmental Chemical Engineering

journal homepage: www.elsevier.com/locate/jece

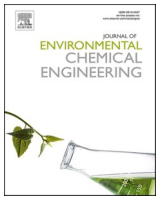

Evaluating hydrothermal liquefaction hydrochar from sewage sludge as a phosphorus resource through struvite production

Shukla Neha [a,b], Leendert Vergeynst [a,b], Patrick Biller [a,b,*]

[a] Department of Biological and Chemical Engineering, Aarhus University, Hangøvej 2, Aarhus N DK-8200, Denmark
[b] Aarhus University Centre for Water Technology (WATEC), Aarhus University, Ole Worms Allé 3, Aarhus C 8000, Denmark

ARTICLE INFO

Keywords:
Sewage sludge
Hydrothermal liquefaction
Hydrochar
Phosphorus
Struvite

ABSTRACT

Hydrothermal liquefaction (HTL) has attracted considerable attention for valorizing sewage sludge to biofuels while the solid residue, hydrochar, has received little attention for its final application. In the current work hydrochar recovered from hot separation in a pilot-scale HTL plant is evaluated for its nutrient value, in particular as a sustainable Phosphorus (P) resource. Following thorough characterization of the hydrochar, P recovery as struvite ($NH_4MgPO_4{\cdot}6H_2O$) is investigated to produce a fertilizer with a lower heavy metal content that could be used in current agricultural practices. P extraction using inorganic (hydrochloric and sulphuric) and organic (citric) acids is evaluated by applying 0.1–1 mol/L of acids for 1–12 h with a liquid/solid ratio of 10 mL/g. A second-order polynomial model was established by response surface methodology (RSM) to predict the P extraction with different acids. The optimum operating conditions for maximum P extraction (94 %) are suggested as 0.7 M of acid strength (H_2SO_4) and 6.5 h of extraction time. Addition of citric acid (CA) during the struvite precipitation from acid-leached P solution was found to improve the struvite purity from 36.6 % to 54 % with a reduction in heavy metal content. Furthermore, morphological analysis validated the formation of struvite. Upon comparison with the regulations, hydrochar was found to exceed some of the heavy metal limits but was low in polyaromatic hydrocarbons (PAHs), per- and polyfluorinated substances (PFAS) and showed low toxicity to *Aliivibrio fischeri*. P extraction and struvite precipitation are shown to reduce heavy metal contents below regulatory limits with P recoveries from 40 % to 67 %. Thus, as an alternative to direct land application of hydrochar, harvested struvite from hydrochar could be applied as a fertilizer with no apparent environmental risk.

1. Introduction

In recent decades, the annual generation rate and amount of sewage sludge from wastewater treatment plants (WWTPs) has increased rapidly due to urbanization and industrialization. In the European Union, approximately 11 million dry tons of sewage sludge are produced per year [1]. The total amount of sewage sludge generated worldwide has increased dramatically, and this trend is expected to continue in years to come. Worldwide, large amounts of sludge are generally disposed of on land. Even though sewage sludge contains valuable nutrients such as nitrogen, phosphorus (P), organic matter, and essential trace elements, which can improve soil physical properties and increase the yields of many crops as effective fertilizers, it can damage the environment when applied directly to soil [2]. It leaches out hazardous substances, both organic and inorganic, including micro-pollutants, polycyclic aromatic hydrocarbons (PAH), and heavy metals into the soil. Other major environmental concerns are associated with the emergence of microplastics (<5 mm) and per- and polyfluoroalkyl substances (PFAS) which have received increasing attention, given their threats to ecosystems and public health [3,4]. In Denmark for example an average of 11 μg/kg PFAS (PFOA, PFOS, PFNA, and PFHxS) were reported in sludge received from 38 WWTPs. In Norway, 18 major WWTPs detected PFAS concentrations ranging from 2.63 to 168 μg/kg in digested sludge [5]. These pollutants exhibit strong biological toxicity, which can cause serious threats to humans, wildlife, and the environment. Therefore, several countries have banned the use of sewage sludge for land applications as it possesses severe health risks. Other alternatives such as disposal in landfills lead to the production of leachate and CO_2 emissions [6] and does not recover the fertilizer value of the sludge. The other practiced technique, anaerobic digestion shows several

* Corresponding author at: Department of Biological and Chemical Engineering, Aarhus University, Hangøvej 2, Aarhus N DK-8200, Denmark.
E-mail address: pbiller@bce.au.dk (P. Biller).

https://doi.org/10.1016/j.jece.2024.113014
Received 16 January 2024; Received in revised form 3 April 2024; Accepted 6 May 2024
Available online 9 May 2024

constraints like large area requirement, odor issues, long active duration (2–4 weeks) and the release of toxic gases such as ammonia, methane, hydrogen sulphide, and nitrous oxide. Additionally, anaerobic digestion does not completely solve the sewage sludge disposal problem as it still leaves a solid residue with the presence of anoxic/anaerobic zones in the solid residue matrix and emerging micropollutants are not destroyed leading to their subsequent release to the environment when the digestate is applied as fertilizer.

On the other hand, thermo-chemical techniques such as combustion, incineration, gasification, pyrolysis and hydrothermal liquefaction (HTL) have attracted increasing attention for sewage sludge management along with the generation of valuable end products viz liquid (oil), non-condensable gases (gas), and solid residue (hydrochar) over the past decade. The high temperatures applied in these processes allow the destruction of many of the concerning micropollutants [7]. However, the high moisture content of sewage sludge (> 95 wt%) makes combustion, incineration, gasification and pyrolysis non-economical due to large energy requirements for drying. Life cycle assessment (LCA) showed that incineration, gasification and pyrolysis possessed net global warming potential in the form of 129–800, 50–3183, 181–385, 80–364 kg CO_2 equivalent per ton of total solid sewage sludge (CO_2eq/t SS_{dry}), respectively [8–11], while HTL showed a comparatively lower carbon footprint (maximum of 172 kg CO_2eq/t SS_{dry}) [12]. HTL was found beneficial for producing high energy density fuel (HHV of 25–40 MJ/kg) from wet biomass such as sewage sludge [13]. The oil produced from HTL can be utilized in boilers and engines for heat and power generation and can be converted to transportation fuel by upgradation processes. There have been several suggestions in the literature for the utilization of HTL hydrochar, including as a solid fuel in boilers, as activated carbon, carbon nanotubes, and nutrient storage media source after catalytic pre-treatment [14]. Their properties concerning surface adsorption sites, surface area (up to 874 m^2/g, [15]) with high porosity, high pH value, and cation exchange capacity have led to research into their utilization as adsorbents to remove organic and heavy metals contaminants from the aqueous phase, soil remediation agent to improve fertility, carbon sequestration, and heavy metals immobilization [16]. Nevertheless, the final application of HTL hydrochar in future commercial endeavours is currently a large question mark. This research gap has been thoroughly summarized and evaluated in a recent review paper by Middelton-Smith et al. from the Pacific Northwest National Laboratory (PNNL) HTL research team [17], encouraging the research community to evaluate the hydrochar in more detail for its final application including the recovery of valuable P as fertilizer.

Several studies have shown P extraction from HTL hydrochar of sewage sludge, chicken and swine manures, food waste, digestate, microalgae etc [18,19]. Thomsen et al. [7] demonstrated 60–100 % P recovery in hydrochar obtained from HTL of fat, oil and grease, food waste, primary and secondary sludge and digestate with no apparent effect of HTL operating conditions in batch reactors. Following HTL, heavy metals in addition to nutrient elements are equally concentrated in the hydrochar in comparison with the feedstock due to the substantial reduction of the quantity of hydrochar generated vs the equivalent feedstock. This could lead to further purification requirements of hydrochar before direct land application. In line with this, struvite ($NH_4MgPO_4 \bullet 6H_2O$), a marketable fertilizer was found as a promising approach to effectively recover P and decrease the heavy metal content [20]. Compared to synthetic P fertilizer, struvite recovered from WWTPs showed lower cadmium and other heavy metal concentrations [21]. Ovsyannikova et al. reported 66–99 % phosphorus (P) recovery as struvite from the HTL byproduct of manure and sewage sludge (hydrochar and process water) [19]. In that study, phosphate was first transformed from HTL solids into liquid through acid extraction and then it led to the precipitation of phosphate salt by adding ammonium-rich HTL process water and an additional Mg source. In previous studies, the effect of operating parameters such as Mg to P ratio, availability of phosphate affecting ions, pH etc. were optimized for maximum P recovery in the form of struvite. However, the effect of acid type and optimization of leaching time and acid strength for maximum P recovery from HTL hydrochar for eventual precipitation of struvite is unexplored.

The current study aims to address some of the existing research gaps, particularly in the understanding of hydrochar recovered using hot separation in continuous HTL reactors, its characterization and its potential as P fertilizer. Following a thorough characterization of the hydrochar, P extraction is evaluated based on the acid type (inorganic and organic) and adjustment of operating parameters. Subsequently, two different struvite precipitation methods (with/without the addition of citric acid) are employed using the HTL process water as a $NH4^+$ source to evaluate total P recoveries, fate of heavy metals and morphology of the final product.

2. Materials and methods

2.1. Materials

The HTL end products (hydrochar and process water) used in this study were produced at Aarhus University in Denmark using a continuous pilot-scale HTL reactor. Primary and secondary sludge from the wastewater treatment plant of Fredericia Spildevand og Energi (Fredericia, Denmark) was used as received in the same proportions as produced at the WWTP of 29 % primary sludge, 71 % secondary sludge, based on dry weight. The HTL reactor has a feed capacity and a total volume of the system of up to 100 L/h and ~20 L respectively. The mixed sludge had a dry matter content of 12 % and was processed at 325 °C at a flow rate of approximately 50 L/h. The hydrochar was recovered in-line at the hottest section of the reactor (325 °C) using a settler where the heavier char particles settled and were continuously recovered as an aqueous char mixture. This approach limits the contact of the HTL hydrochar with the produced bio-crude due to density differences and avoids additional solvent extraction or cleaning steps of the HTL hydrochar. Although the yields of end products were not quantified for this HTL run, an identical sludge composition underwent the HTL process in batch reactors under the same conditions (325 °C ~20 min) resulting in 33 % biocrude, 24 % hydrochar, 34 % aqueous phase, and 9 % gas [7]. Thus, it is expected that the continuous reactor operation using the same sludge yielded a similar mass balance. Hydrochar received from the HTL reactor was dried in an oven at 105 °C overnight and grounded afterwards to powder form. Organic contamination of the hydrochar was assessed by washing it overnight with dichloromethane (DCM) and water separately (1 g/10 mL) to extract biocrude and water-soluble organics originating from the HTL process water, respectively. Received water from hydrochar leaching was further subjected to toxicity analysis. Process water was characterized and subsequently stored in a fridge at 5 °C prior to use. Hydrochloric acid (HCl), sulphuric acid (H_2SO_4), citric acid (CA), sodium hydroxide (NaOH) pellets (≥85 %), magnesium chloride ($MgCl_2{\cdot}6H_2O$) and commercial struvite (magnesium ammonium phosphate, $MgNH_4PO_4.6H_2O$) were purchased from Sigma Aldrich, Denmark. As per the experimental requirements, the strength of the acids (HCl, H_2SO_4, CA) were maintained by dilution.

2.2. Nutrient extraction

Hydrochar utilization was analyzed for its nutrient extraction, with inorganic (HCl and H_2SO_4) and organic (CA) acids, where acid strength and extraction time were varied to obtain maximum P extraction. 10 mL of a leaching agent (acid) having different strengths was added to 1 g of the dry hydrochar. The resultant acid-hydrochar solution (nutrient-leached acid) was stirred magnetically (500 rpm) for different periods and later filtered with a 13 μm filter paper. The leaching capacity for P/nutrients was calculated from the amount of the P/nutrient that was extracted in leachate divided by the hydrochar mass, as per Eqs. (1) and (2).

$$M_L = C_{leachate} \times V_{leachate} \quad (1)$$

$$E = \frac{M_L}{M_{hydrochar} \times C_{hydrochar}} * 100 \quad (2)$$

Where M_L is the mass of P/nutrient in leachate (mg), $C_{leachate}$ is the concentration of the P/nutrient in leachate (mg/L), $V_{leachate}$ is the volume of the leachate (L), E is the extraction percentage (%), $M_{hydrochar}$ is the mass of the hydrochar (g) and $C_{hydrochar}$ is the concentration of P/nutrient in hydrochar (mg/g).

2.3. Statistical design of experiment

Central Composite Design (CCD) is a common form of response surface methodology which is used to design experiments. CCD provides valuable insights into complex systems and processes while requiring a relatively small number of experimental runs compared to other design methods such as Box-Behnken Design, Optimal design, full factorial etc [22]. CCD enables the modeling and optimization of processes with multiple variables and establishes the dependability between factors and responses more comprehensively. This approach aids in optimizing processes, reducing costs, and accelerating the development of solutions. The CCD model considers mutual interactions amongst the factors that impact P extraction. Design Expert® software was used to analyze the experimental responses in order to identify the operating parameters which impact the P extraction from the hydrochar. A set of 11 experimental runs were carried out for each individual acid (HCl, H_2SO_4, CA) using the predetermined range of two operating parameters viz, acid strength (0.1–1 M) and extraction time (1–12 h) (Table S1) at five levels (0, ± 1 and ± α), with the higher and lower levels selected based on previous studies [19,23]. All experiments were performed as per the designed runs and P extraction (%) was taken as the response. Subsequently, regression analysis was conducted to develop a second-order polynomial model to describe the experimental results. The factors having a confidence level higher than 95 % were considered sufficiently significant for P extraction. Statistical analysis of the experimental run was done with the analysis of variance (ANOVA) and the multiple regressions by Design Expert 7.1.6 statistical software.

2.4. Struvite precipitation

Nutrient-leached acid, showing the highest P extraction under optimized operating conditions from Section 2.3 was used for struvite precipitation. 10 mL of nutrient-leached acid was mixed with $MgCl_2.6H_2O$ and HTL process water (NH_4^+ source) in the respective Mg:P and NH_4^+: P ratio of 1.6:1 and 2.6:1, to guarantee an oversaturation state for struvite crystallization. Compared to Mg, NH_4^+ ion concentrations were kept high for better struvite purity [19]. Accordingly, with 1 M NaOH, the pH of the solution was maintained up to 9 and stirred for 2 hours (at room temperature) in order to achieve crystallization. Subsequently, the solution was filtered with 13 μm filter paper and the precipitated struvite (hydrochar struvite) was kept overnight for dying (at 35 °C). To promote struvite precipitation and to control the effect of metal ions such as Al, Fe, and Ca, citric acid (CA) was added to nutrient-leached acid for 10 min [19]. Thereafter, $MgCl_2.6H_2O$ and HTL process water were added in the previously mentioned ratio, accordingly the pH was increased to 9 and again, the experiment was conducted identically to the one described above. Received struvite was named as CA-hydrochar struvite. The purity of struvite was calculated as per Eq. (3) [24], where NH_4^+ concentration was calculated by dissolving hydrochar struvite, and CA-hydrochar struvite in HNO_3. All the experiments were conducted twice, and reproducibility was expressed through standard deviation.

$$struvite\ purity = \frac{n_{NH_4^+} \times M_{struvite}}{m_{precipitate}} * 100\% \quad (3)$$

Where, $n_{NH4}+$, $M_{struvite}$ and $m_{precipitate}$ are the moles of NH_4^+ in the precipitate (mol), molar mass of struvite (g/mol) and precipitate mass (g), respectively.

2.5. Analysis techniques

Nutrients present in hydrochar, HTL process water, nutrient-leached acid, hydrochar struvite, CA-hydrochar struvite and commercial struvite were analyzed using an inductively coupled plasma-optical emission spectrometer (ICP-OES, Agilent 715). The procedure for solid and liquid samples analysis is described by Matayeva et al. [18]. The samples were analyzed for P, Mg, Ca, K, Na, Zn, Fe, Cr, Al, Cu, Ni and Mn contents. The ammonium content of the HTL process water and nutrient-leached acid was determined by the Merck Spectroquant cuvette tests (NH_4^+-114559) [25]. The pH of the liquid samples was measured with a portable meter (Knick Portavo 907). Availability of the functional groups in hydrochar, hydrochar struvite, CA-hydrochar struvite and commercial struvite were analyzed with Bruker Alpha Platinum Attenuated Total Reflectance Fourier-transform infrared spectroscopy (ATR- FTIR) spectrometer. From FTIR, a total of 24 spectra from 4000 to 400 cm^{-1} were collected with a resolution of 2 cm^{-1}. X-ray diffraction (XRD) data was collected using a Panalytical Aeris diffractometer equipped with a PIXcel1D detector in Bragg-Brentano geometry, using Cu Kα1 (1.54056 Å) and Kα2 (1.54439 Å) radiation. (keV 40, 15 mA). Measurements were made over 300 minutes per sample, using a flat, low-background silicon sample holder. Scanning electron microscopy (SEM) images and Energy dispersive X-ray spectroscopy (EDS) were acquired using a Tescan Clara scanning electron microscope equipped with a 4Q-BSE detector. Compositional maps were produced by collecting data from 3 regions of each sample after extracting data from AZtec software (Oxford Instruments). Thermogravimetric analysis (TGA) was done to determine moisture, volatile matter, fixed carbon, and ash content of solid samples using a Mettler Toledo TGA-DSC3+ (Germany). The samples were heated from 50 °C to 900 °C at 20 °C/min in N_2 and then air was introduced for 20 min. The toxicity of hydrochar was evaluated from the overnight extraction of hydrochar in water using the BioTox assay (Aboatox Oy), which measures acute (15–30 min) bioluminescence inhibition of the bacterium *Aliivibrio fischeri*, following the ISO standard 21338 [26]. Samples and dichlorophenol as reference inhibitors were analyzed in triplicate from a 2-fold dilution series. PFAs concentration in hydrochar was quantified by the external contract laboratory Eurofins Miljø A/S Ladelundvej Vejen, Danmark.

3. Results and discussion

3.1. Characterization of HTL hydrochar

The mixture of primary and secondary sludge prior to HTL exhibited a C, H, N, S, O content of 37.9 %, 5.4 %, 6.5 %, 0.8 % and 27.3 % respectively, with an ash content of 22.1 % and a P concentration of 20,140 mg/kg. Focusing on the produced hydrochar; upon washing with water and DCM, 1.2 % and 2.5 % mass loss was observed, respectively and no color was leached in both cases. Thus, it can be concluded that the hydrochar recovered from the HTL plant is reasonably clean and ideally can be utilized without further modification. Table 1 shows the properties of the HTL hydrochar. Proximate analysis shows that hydrochar comprises 0.5 wt% moisture, 25 wt% volatile matter, 4.5 wt % fixed carbon and 70 wt% ash. The ultimate analysis revealed 21.4 wt % C, this low C and fixed carbon of hydrochar is due to its separation at hottest reaction condition which prevents the re-polymerization of reaction intermediates [27]. Previous work on recovery of hydrochar from manure using hot separation in a continuous HTL reactor [7,27] also showed low C (~20 wt%) and fixed carbon (~5 wt%). The high ash and low C content revealed that the in-line hydrochar separator of the continuous HTL plant effectively avoids organic impurities and produced a cleaner hydrochar. The hydrochar contained 61,750 mg/kg of

Table 1
Properties of HTL hydrochar.

Proximate and ultimate characteristics (%)	Values	Nutrients and metals (mg/kg)	Values
Moisture content	0.50 ± 0.01	P	61,750 ± 152
Volatile matter	25.0 ± 0.8	Mg	58,170 ± 103
Fixed carbon	4.5 ± 0.2	K	9873 ± 30
Ash content	70.0 ± 2.1	Al	15,450 ± 114
C	21.4 ± 0.8	Fe	5,547 ± 97
H	2.4 ± 0.1	Ca	68,653 ± 147
N	1.70 ± 0.02	Zn	882 ± 25
S	0.40 ± 0.01	Cu	376 ± 14
O	4.1 ± 0.3	Ni	293 ± 3
		Cr	91 ± 2.3

P, 58,170 mg/kg of Mg and 9873 mg/kg of K, but also 882 mg/kg of Zn, 376 mg/kg of Cu, 239 mg/kg of Ni and 91 mg/kg of Cr (Table 1). Toxicity analysis of the hydrochar extract showed a concentration-dependent inhibition of *Aliivibro fisheri* with up to 29 ± 10 % inhibition at the highest level (50 % dilution). As a positive control, dichlorophenol showed a clear concentration-dependent response with a half maximal effective concentration (EC50) of 2.6–4.0 mg/L, which is within the expected range according to the ISO 21338 guideline. Other properties of hydrochar char such as TGA and FTIR are discussed and compared in the upcoming sections. Thus, low C and HHV make hydrochar unattractive for carbon sequestration and incineration, respectively. Whereas the high P content (61,750 mg/kg), permissible limits of PAH (< 6 mg/kg) and PFAS (< 10 μg/kg) in hydrochar showed its commercial potential as an alternative to the dependency on mineral P fertilizers and to utilize hydrochar as a nutrient source. Despite low PAH and PFAS, the elevated heavy metal concentration led to the motivation of subjecting the hydrochar to acid leaching to extract maximum P for further struvite precipitation.

3.2. Effect of operating parameters on P extraction

The effect of acid strength and extraction time on the P extraction from hydrochar is shown in Fig. 1(a) and (b), respectively. P extraction increases with an increase in acid concentration (Fig. 1a). At the concentration of 0.9 M, a maximum of 93.5 %, 81.2 % and 63.0 % of P extraction was achieved with H_2SO_4, HCl and CA, respectively. With further increase of acid concentration, P extraction was stagnant due to the formation of nucleation particles in the matrix of hydrochar. While leftover P could be found as nucleation particles in the centre matrix of hydrochar as well as in the form of insoluble salts. Another possible reason may be explained by the fact that increased acid concentration results in the formation of insoluble $CaSO_4$, which adheres to the surface of hydrochar. This impedes the acid from reaching the inner core of the hydrochar, thereby diminishing the effectiveness of P extraction [28].

The lowest P extraction (63.0 %) with CA is probably due to the formation of secondary apatite phosphate precipitates [28]. Compared to organic acid (CA), inorganic acids (H_2SO_4 and HCl) provided higher P extraction by dissolving alkali-metal oxides and leaching P from organic and inorganic phases, while organic acids enable the release of metals/metalloids and metal-bound P by inducing chelating effects [29]. Hong et al. studied P recovery from waste-activated sludge incinerator ash and found that 2 M of HCl and 1 M of H_2SO_4 could extract 69 % and 98 % of P, respectively [30]. While, Xu et al. reported the highest P extraction efficiency of 99 % with 0.3 M of H_2SO_4, compared to HCl (97 %), citric acid (91 %), and acetic acid (30 %) [28]. The P extraction from hydrochar to nutrient-leached H_2SO_4 could be represented with Eqs. (4) and (5) [31], where strong acids help to overcome the buffering resistance provided by the hydrochar slurry. Stronger acids such as H_2SO_4 having lower pK_a values (-10), help in the dissolution of Al^{+3} and Fe^{+3} ions bound to P in hydrochar as compared to that of HCl (-6.3) and CA (3.12, 4.76 and 6.39). Accordingly, along with P, Al and Fe were also extracted in the nutrient leached H_2SO_4 which can affect the struvite precipitation process (discussed in upcoming Section 3.6).

$$AlPO_4 + 3H^+ \rightarrow Al^{+3} + H_3PO_4 \quad (4)$$

$$Fe(PO_4)_2 + 6H^+ \rightarrow 3Fe^{+2} + 2H_3PO_4 \quad (5)$$

The effect of extraction time on P extraction with H_2SO_4, HCl and CA is shown in Fig. 1(b). P extraction increases with increasing extraction time and eventually reaches the plateau. 94 %, 77 % and 63 % of P extraction was achieved with H_2SO_4, HCl and CA respectively within less than 7 h. Increase in extraction time provides the energy necessary for the breakdown of the chemical bonds of the metals in the hydrochar. Thus, considering the cost-effective consumption of acid and achievement of complete P extraction, 0.7 M of H_2SO_4 for 6.5 h of extraction time was considered the most suitable condition for maximum P extraction.

3.3. Combined effect of operating parameters on P extraction

To evaluate the combined effect of operating conditions on P extraction, a set of acid extraction experiments was conducted according to the experimental runs generated using CCD. The experimental conditions and the P extraction from each experimental run (calculated as per Eq. (2)) are tabulated in Table 2. The highest P extraction (95 %) was obtained with 0.5 M of H_2SO_4 for 12 h of leaching time. While, with CA and HCl, 91 % and 76 % of P were extracted with acid strength and

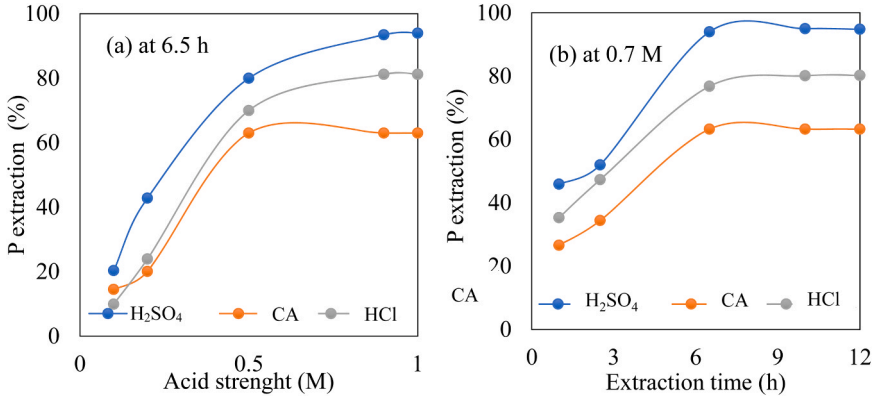

Fig. 1. Effect of (a) acid strength and (b) extraction time on P extraction with different acids.

Table 2
Phosphorus extraction with different acids.

Operating parameters		P extraction (%)		
Acid strength (M)	Extraction time (h)	H_2SO_4	CA	HCl
0.1	6.5	20.3	14.5	9.9
0.5	6.5	89.5	66.0	67.7
0.9	2.5	60.5	50.2	76.9
0.2	2.5	36.3	18.6	17.7
0.5	6.5	89.9	65.2	67.0
0.2	10	48.2	27.4	30.1
0.9	10	90.8	76.1	85.5
1	6.5	59.0	32.4	50.0
0.5	1	65.9	26.6	35.3
0.5	6.5	89.2	66.2	67.5
0.5	12	95.0	71.9	63.2

extraction time of 0.9 M and 10 h. In previous studies, a maximum of 100 %, 98 % and 95 % of P was extracted with H_2SO_4, HCl and CA, respectively, while maintaining acid strength of 1 M and 2 h of extraction time [23,29,32]. Fig. 2(a–c) illustrates the contour plots of P extraction at different operating conditions with different acids. Low acid strength and low extraction time resulted in the lowest P extraction (around 20 %), whereas at intermediate to acid strength (> 0.5 M) and high extraction time (> 6 h), the highest P extraction (~ 95 %) was observed (Fig. 2a). On the other hand, with CA, extraction time of more than 6 h and intermediate acid strength (0.5–0.9 M) resulted in the highest P leaching (76.10 %, Fig. 2b). Even though as a tribasic acid, CA provided more reaction sites and more H^+ at the same time, it solubilized P more efficiently at low molarity compared to inorganic acids. High molarity of organic acids such as CA was unable to complete the dissociation and resulted in reduced P extraction capacity [19]. With HCl, maximum P extraction (86 %) was achieved with high acid strength (> 0.7 M) and high extraction time (> 6 h, Fig. 2c). Improved acid strength and sufficient time provided increased energy for breaking the metal chemical bonds to release P. Accordingly, the suggested optimum condition for the maximum P extraction with different acids is listed in Table 3. Compared to HCl and CA, H_2SO_4 was extracting maximum P (94 %) at an acid strength of 0.7 M for 6.5 h of extraction time. While respective optimized conditions with HCl (maximum 75 % of P extraction) and CA (maximum 68 % of P extraction) were 0.9 M of acid strength 10.4 h of extraction time 0.62 M of acid strength and 6.5 h of extraction time. The highest P extraction with H_2SO_4 was due to the availability of double concentration of H^+ ions. Overall, results from the present study on maximum P extraction are broadly in agreement with studies on P extraction from other P waste resources such as municipal mixed waste compost residue, ashes of sludge incinerators and flyash [33–35] showing the good potential of HTL derived hydrochar as a sustainable P resource.

3.4. Statistical analysis and model validation

A second-order polynomial model was obtained by the regression analysis for predicting the response (P extraction) for H_2SO_4, CA and HCl in terms of acid strength, A (M) and extraction time, T (h) as given in Eqs. 6- 8, respectively. The analysis of variance (ANOVA, Table S2) indicated that the quadratic model for P extraction gives good prediction at a 95 % confidence level. F-value for the model is higher than $F_{0.05}$, rejecting the null hypothesis. The F-value of the suggested models (7.04–8.46) implies that the models are significant, whereas p-values < 0.05 indicate that model terms were significant. The linear terms of A and T for all acids (excluding T for HCl) and quadratic terms of A had a significant effect on P extraction (Table S2). The predicted and adjusted R^2 of the models were in the range of 0.61–0.91 and 0.74–0.97, respectively. Additionally, the coefficient of variation (C.V) < 10 % of the model (4.43–5.50 %) indicated low variation from the mean value and reproductivity of the model. Besides the identification of the outliers

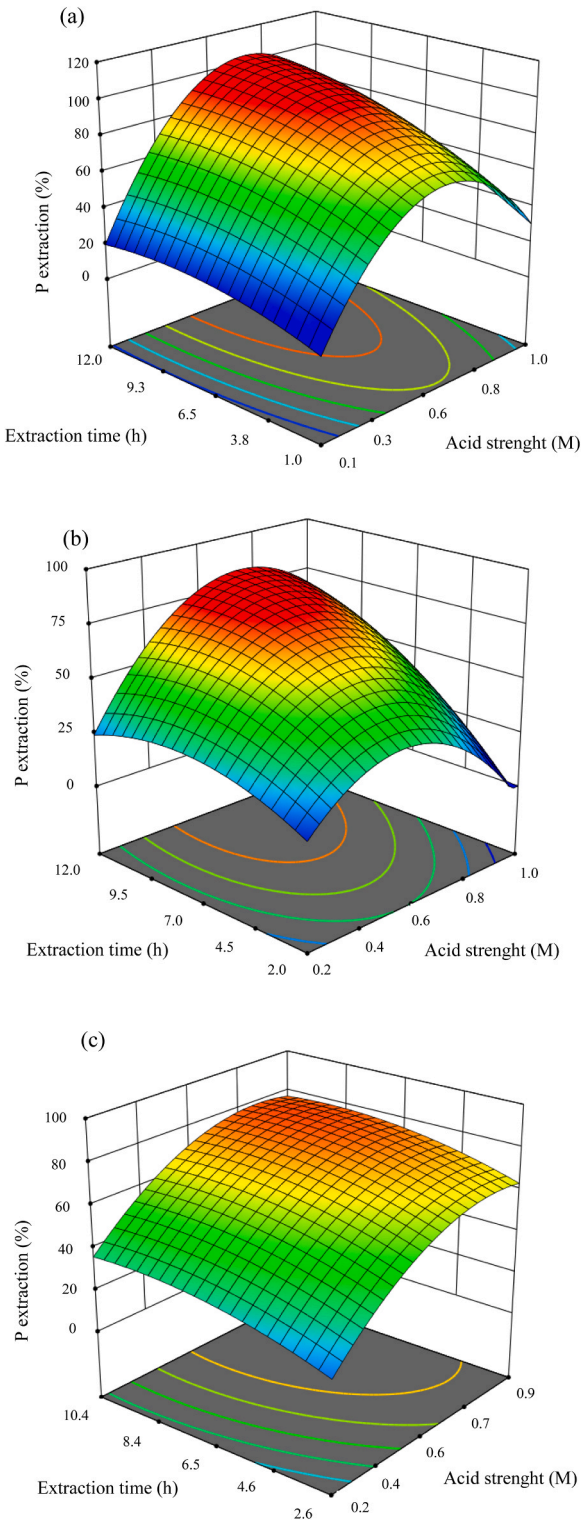

Fig. 2. Effect of temperature and extraction time on P extraction with (a) H_2SO_4, (b) CA and (C) HCl.

Table 3
Optimized conditions for maximum P extraction.

Parameters	H_2SO_4	CA	HCl
P extraction (%)	94.0	67.5	75.3
Acid strength (M)	0.69	0.62	0.86
Extraction time (h)	6.5	10.4	10.4

by externally studentized residuals for different acids showed that the residuals were lying within the acceptable range (± 5.67 value of the outlier) (Fig S1 (a–c)).

$$\text{P extraction } (H_2SO_4) = -24.67+299.03\ A +4.04\ T +3.54\ AT -251.01\ A^2 -0.24\ T^2 \quad (6)$$

$$\text{P extraction (CA)} = -30.38+205.61\ A+5.90\ T+8.16AT- 206.98\ A^2- 0.47\ T^2 \quad (7)$$

$$\text{P extraction (HCl)} = -43.19 +237.80\ A +7.26\ T -0.52\ AT -152.55\ A^2 -0.38\ T^2 \quad (8)$$

Based on the optimization outcomes, H_2SO_4 was selected to extract maximum P (94 %) under optimized operating conditions (0.7 M of acid strength and 6.5 h of extraction time). Further, to check the applicability of the obtained model (R^2 of 0.98) for maximum P extraction, the model was validated with higher H_2SO_4 strength (up to 3 M) and longer extraction time (up to 12 h) (Fig S2 (a-b)). A rapid increase in P extraction (up to 78 %) was observed up to 0.5 M of acid strength. After that, 20 % increment in P extraction was obtained while increasing acid strength up to 1 M (Fig S2 (a)). On the other hand, up to 2.5 h of extraction time, 53 % of P was extracted. While 6.5 h of extraction time showed a maximum P extraction of 94 %. Further increase in extraction time didn't show any significant increase in P extraction (Fig S2 (b)).

3.5. Struvite production from nutrient-leached acid

Based on the optimization studies for maximum P extraction, nutrient-leached H_2SO_4 (0.7 M for 6.5 h of extraction time) was subjected to struvite precipitation. Nutrient-leached acid contained 58,045 mg/kg of P, 54,210 mg/kg of Mg, and 365.4 mg/kg of NH_4^+. To maintain the required Mg:P (1.6:1) and NH_4^+: P (2.6:1) ratio for struvite precipitation, extra NH_4^+ (27.88 mL of HTL process water per g of hydrochar((1500 mg/L of NH_4^+ and 400 mg/L of P)) and Mg (0.154 g of $MgCl_2$ per g of hydrochar) was added to the nutrient leached H_2SO_4. Subsequently, the pH was adjusted to 9 and struvite was precipitated. Fig. 3 illustrates the overall P mass balance, although the HTL mass balance was not performed for this exact pilot scale production run, the P balance data from a corresponding identical batch HTL experiment using the same conditions and sludge [7] was used for the first part of the overall mass balance. From 100 g of P-sewage sludge, HTL sequestered 99 g of P to the hydrochar (Fig. 3(a)) (based on previous P balance). Acid leaching resulted in 93 g of P extraction in nutrient leached acid from sewage sludge leaving 6 g in the spent hydrochar and 1 g in process water. During precipitation, the addition of process water supplemented 0.11 g of P. Despite a 82 % struvite weight yield, the precipitate (hydrochar struvite) only showed a purity of 36.6 % resulting in an overall P yield of 67 % from sewage sludge to struvite. This low purity was due to the co-precipitation of other heavy metals. The presence of Ca, Mg, NH_4^+, and PO ions in hydrochar and nutrient leached acid formed ion complexes such as $Ca_3(PO_4)_2H_2ONH_3$, $CaHPO_4$, $Ca_3(PO_4)_2NH_4^-$, $Mg_3(PO_4)_2$, $MgHPO_4$, $MgOH^+$, H_3PO_4, $H_2PO_4^-$, HPO_4^{-2}, $MgNH_4PO_4$, $MgPO_4^-$, $MgH_2PO_4^+$, $MgHPO_4$ etc by dissociation, complexation, precipitation and crystallization reaction [36]. Excess availability of these ions increases the ionic strength of the solution and significantly reduced the P extraction and struvite purity by lowering Mg^{+2} activity [37].

Struvite precipitation could be expected via two major mechanisms: nucleation and crystal growth. At the beginning of the reaction, the

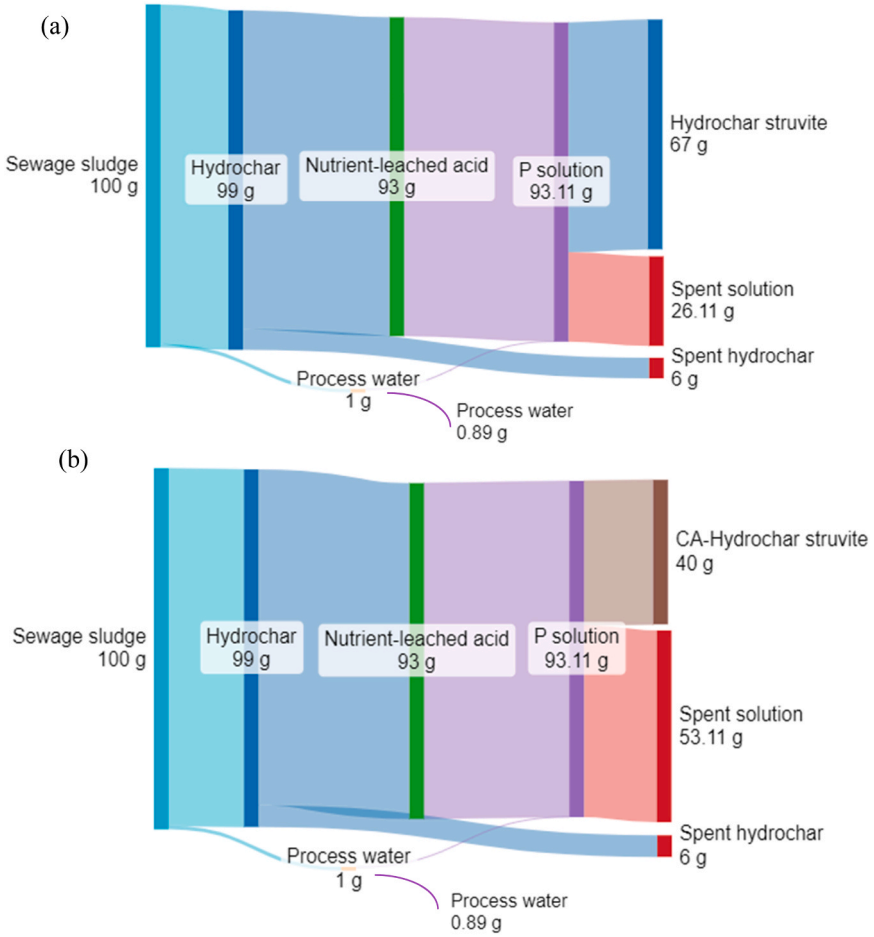

Fig. 3. P mass balance from sewage sludge to (a) hydrochar struvite and (b) CA-hydrochar struvite.

struvite crystal nuclei is formed via nucleation. These nuclei agglomerate and grow over time, during which heavy metal hydroxide might be the main species of heavy metal precipitation. When the ionic activity product of the struvite components exceeds the solubility product of struvite, the precipitation reactions occur [38]. During the precipitation of struvite, the liberation of H^+ occurred along with the expense of Mg^{+2} [39]. Due to the high availability of substantial functional groups (hydroxyl groups, ammonium groups, and phosphate groups), heavy metal precipitates are eventually formed and then adsorbed on the surface of struvite through coordination bonding. Supposing, the crystallization rate of heavy metal precipitates is much lower than struvite crystals, heavy metals might not affect the internal structure and composition of struvite. However, the high presence of heavy metals can reduce the crystallization rate of struvite. Heavy metal ions could be adsorbed onto crystal surfaces during nuclei development thus inhibiting the crystal growth [40].

Addition of CA promoted P recovery and inhibits heavy metal precipitation. As a result, the struvite purity increased up to 54 % with a reduction in the struvite weight yield from 82 % to 36 % which eventually lowered the P yield to 40 g from 100 g of P-sewage sludge (Fig. 3 (b)). Reduction in struvite weight is due to the increase in the diffusion coefficient of the solution with extra CA and the reduction in impurities which may inhibit the formation of struvite crystals. The higher purity of struvite produced in the presence of CA however led to a lower total P yield from sewage sludge to struvite of only 40 %. CA-hydrochar struvite showed reduced contents of Al, Fe, Ca, Zn, Cu and Cr by 74 %, 33 %, 97 %, 72 %, 89 % and 91 %, respectively to that of hydrochar as shown in Table 4. The biodegradable complexing quality of CA formed stable soluble complexes with Al, Ni, Fe, Ca, Zn, Cu, and Cr cations present in nutrient-leached acid and made metal cations inaccessible for precipitation and binding with phosphate ions [40], which dropped the metal concentration drastically and improved the struvite purity. Another possibility is that CA may inhibit the formation of Mg–N–P nuclei, while the generation and growth rate of heavy metal–N–P and heavy metal –OH nuclei is significantly promoted. As a result, the formed heavy metal –N–P and heavy metal–OH nuclei may become seeds for further struvite formation. Reduction in heavy metals in CA-hydrochar struvite indicated that it may have a significant effect on the change of struvite crystal growth rate. Transformation of HPO_4 to PO_4 at high pH and increment in solution supersaturation could be the reason for favorable struvite formation [41]. These observations indicate the efficacy of CA for controlling Al, Fe, and Ca ions in the solution and benefiting struvite formation. It should be noted that Warmadewanthi et al. [42], Wang et al. [43] and Siciliano [44] reported 68 % 88 % and 96 % of phosphate conversion from landfill leachate into struvite, respectively. Becker et al. recovered 80 % of P in the form of struvite (precipitate yield of 56 %) from hydrothermal carbonized hydrochar of sewage sludge [45], while Numviyimana et al. achieved 99.96 % P recovery as struvite from hydrothermal carbonization liquor of chemically produced dairy sludge [46]. Ovsyannikova et al. reported reduction in P recovery from 95 % to 46 % with CA addition due to the selective adsorption and binding of free CA to the faces of the struvite with a high density of Mg and NH_4^+ cations [19]. The same observation has been made here, with the reduced P recovery, presenting a trade off between increased purity and higher P recovery. These results hence show that it should be possible to improve the P recovery as struvite from the leachate also in the current study by further process optimization.

3.6. Characterization of hydrochar struvite

Even though hydrochar struvites showed the presence of the required chemical composition of struvite (P, Mg, N and O); the existence and purity of struvite crystal were further confirmed by morphological properties such as XRD, SEM-EDS and FTIR spectrum in terms of crystalline phases, spatial arrangements and available functional groups, respectively. The XRD spectrograms of hydrochar struvites are shown in Fig. 4(a). Hydrochar struvite shows no composition of crystalline peaks. Compared to the peaks of commercial struvite, low peak intensities of hydrochar struvite showed the existence of amorphous impurities. While peaks of CA- hydrochar struvite were identical and overlapping to those of commercial struvite in the form intensities, corroborating those reported by other researchers [40,48,49]. Enhancement in the peak intensity at 2θ of 15–17°, 21–22°, 27° and 30° could be demonstrated by the formation of lattice planes of the struvite [36,37]. Availability of calcite and amorphous calcium phosphate was confirmed by the small peaks at 28°, 40°, 43°, 47° and 30°, respectively [38]. SEM image of hydrochar struvite (Fig. 4(b)) showed that it is mostly amorphous and coarse with an irregular powder shape. Compared to hydrochar, hydrochar struvite was found in agglomerated powder form. Along with precipitates of struvite, precipitation of counter ions like Ca, Zn, Cu, etc (Fig S3) formed Ca-phosphate compounds (hydroxyapatite), hydroxides, and oxides in irregular small particles over the surface of hydrochar struvite precipitates [39]. These foreign deposits were spherical, which made them easily coagulate from the nutrient-leached acid solution. While CA-hydrochar struvite crystal showed some regular needle-shaped crystalline products and smooth surfaces. CA promoted nucleation, aggregation and growth rate of crystals into two main forms: distinctive orthorhombic structure and needle-like structure with different thicknesses and lengths [50]. Accordingly, it was comparable to an X-shaped dendritic envelope and rectangular-like structure of commercial struvite. Overall, it appeared that the addition of CA not only significantly affected the morphology of struvite but also effectively promoted the crystal growth of struvite.

The functional groups in hydrochar, hydrochar struvite and CA-hydrochar were identified with the FTIR spectrum in Fig S4 and compared to that of commercial struvite. Hydrochar showed stretching of symmetric bending vibration of PO_4 at 421 cm^{-1} and asymmetric bending vibrations of PO_4 at 508 cm^{-1}. Also, small symmetric stretching vibrations and asymmetric stretching vibrations of PO_4 were observed at 1023 cm^{-1} and 1067, respectively. CA-hydrochar struvite showed prominent symmetric bending vibration of PO_4 at 421 cm^{-1}, asymmetric bending vibrations at 508 cm^{-1} and the wagging modes of

Table 4
Comparative analysis of hydrochar struvites.

Parameters	Hydrochar	Nutrient leached Acid	Hydrochar struvite	CA-hydrochar struvite	Commercial struvite	EU limit [5,47]
Yield (wt%)	-	-	82.9 ± 1.8	36.4 ± 2.0	-	-
P (mg/kg)	61,750 ± 152	58,045 ± 75	50,910 ± 145	67,400 ± 168	125,700 ± 157	-
Mg	58,170 ± 103	54,210 ± 55	30,850 ± 99	55,500 ± 112	107,800 ± 85	-
Struvite purity (%)	NA	-	36.6 ± 0.3	53.8 ± 1.2	NA	-
Al (mg/kg)	15,450 ± 114	14,621 ± 12	11,425 ± 95	2,863 ± 87	2.30 ± 0.2	-
Fe (mg/kg)	5,547 ± 97	4,678 ± 17	4,334 ± 105	3,674 ± 112	13.54 ± 1.9	-
Ca (mg/kg)	68,653 ± 147	59,668 ± 20	6,205 ± 51	1,538 ± 45	883.3 ± 68	-
Zn (mg/kg)	882 ± 25	764 ± 10	687 ± 25	240.9 ± 14	NA	300
Cu (mg/kg)	376 ± 14	119 ± 5	112 ± 10	40.6 ± 1.8	NA	140
Ni (mg/kg)	293 ± 3	105 ± 3	42 ± 2	15 ± 0.7	NA	50
Cr (mg/kg)	91 ± 2.3	32 ± 1.5	24 ± 5	7.13 ± 0.8	2.3 ± 0.5	95

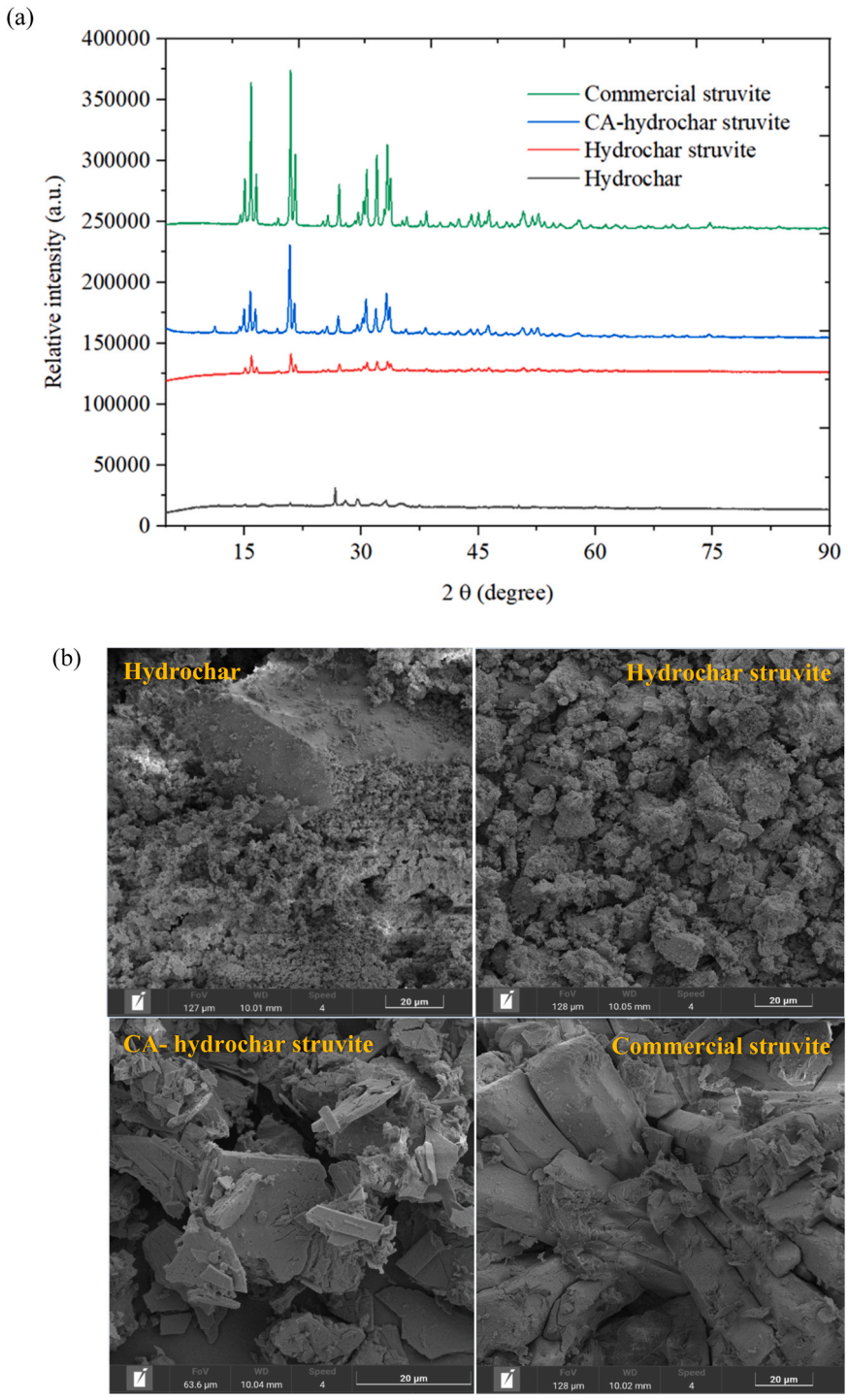

Fig. 4. (a) XRD and (b) SEM of hydrochar struvite.

vibration of coordinated water at 894 cm^{-1} while those at 494 and 572 cm^{-1} are attributed to metal-oxygen bonds. At 1023 cm^{-1}, symmetric stretching vibration of PO_4 and at in the range of 1067–1239 cm^{-1}, availability of cation asymmetric stretching vibrations of PO_4 units were prominent. Additionally, H – O – H bending and stretching were exhibited at 1500–1700 cm^{-1} (with a peak around 1640–1650 cm^{-1}) and 2700–3800 cm^{-1}, respectively. The presence of the above-mentioned functional groups is comparable with the commercial struvite while, on the other hand, hydrochar struvite showed weak peaks of the same. The availability of these PO_4 and OH groups is in line with the previous literature on struvites [51,52].

The elemental composition of hydrochar struvite differs with the addition of CA, accordingly, a 150 %, 24 %, 38 % and 143 % increase in C, H, N and O with 42 % and 21 % decrease in S and ash content were observed respectively (Table 5). Enhanced C and O % were due to the addition of CA [41] while increments in H and N % corresponded to the NH_4^+ from process water. These findings were also corroborated by the EDS analysis (Table S3). Based on the correlation between FTIR peaks and elemental analyses, CA-hydrochar struvite could be called a mixture of struvite and amorphous coprecipitates (with the main part composed of amorphous coprecipitates). The amorphous co-precipitates can be described as Al, Fe phosphate and Ca-containing compounds. Moreover,

Table 5
Elemental composition and molar ratio of hydrochar and hydrochar struvite.

		Hydrochar	Hydrochar char struvite	CA- hydrochar struvite	Commercial struvite
Elemental Composition (%)	C	21.35	3.45	8.64	0.21
	H	2.43	3.88	4.83	5.86
	N	1.69	3.00	4.14	5.51
	S	0.41	1.07	0.62	0.03
	O	4.12	7.1	17.27	6.39
	Ash	70.0	81.5	64.5	82
P: N:Mg	(wt%)		5.09: 3.00: 3.08	6.74: 4.14: 5.55	12.6: 5.7: 9.9*
	Molar Ratio		1.0: 1.3: 0.7	1.0: 1.3: 1.0	1.0: 1.0: 1.0*

* Theoretical value.

hydrochar struvite demonstrated an elemental molar ratio of 1.0: 1.3: 0.7 (P: N: Mg) while CA- hydrochar struvite showed an improved ratio of 1.0: 1.3: 1.0 similar to the theoretical value 1: 1: 1 (Table 5). The higher P and N to Mg ratio could be due to the formation of non-struvite compounds such as ammonium hydroxide (NH_4OH), ammonium phosphate ($(NH_4)_3PO_4$), diammonium phosphate ($(NH_4)_2HPO_4$), ammonium dihydrogen phosphate ($NH_4H_2PO_4$) and dittmarite ($Mg(NH_4)(PO_4)H_2O$) etc [53]. Production of the above NH_4^+ formation and struvite reactions are quite competitive and primarily depends on the concentration of other available ions [5]. It is evident from these findings that the addition of CA provided a more pure form of struvite in terms of high P content.

The thermal behavior of the hydrochar and produced struvite is shown in Fig. 5 with the TGA/DTG curves. TGA revealed decomposition in three stages, (1) moisture removal & release of small volatiles, (2) volatilization & thermal degradation and (3) formation of fixed carbon. In the first stage, up to 105 °C, hydrochar lost 0.9 % of weight, while hydrochar struvite and CA-hydrochar struvite lost 25 wt% and 32 wt%, respectively. The initial mass loss of hydrochar was due to moisture evaporation. Weight loss in hydrochar struvite and commercial struvite in this stage was due to the simultaneous liberation of the water and ammonia to $MgHPO_4H_2O$ with a molecular ratio of 5:1 [50]. Similar results were reported in previous studies showing 45 wt% reduction within 100 °C of thermal decomposition [39,54]. DTG curve shows a sharp peak at 90 °C indicating the faster release of ammonia and part of crystal water. The release of water and ammonia could be explained by the fact that compared to magnesium–water oxygen (2.081 Å) and phosphorus–oxygen (1.543 Å), crystal water bond energy is the weakest and NH_4^+ groups do not enter into the crystal lattice of struvite [55]. In the temperature range of volatilization and formation of fixed carbon (105–900 °C), i.e., in the second and third stages, hydrochar lost 20 % of weight with a DTG peak at 225 °C and 900 °C due to devolatilization and char combustion. Hydrochar struvite and CA-hydrochar struvite reduced 20 % and 30 % of weight respectively due to the elimination of volatile organic species [39]. In a similar temperature range, commercial struvite showed 18 % weight reduction. This could be due to the formation of water vapour and struvite residues of Mg-pyrophosphate ($Mg_2P_2O_7$) and magnesium phosphate ($Mg(PO_4)_2$)[40]. Compared to hydrochar (70 %), hydrochar struvite showed 17 % less ash content due to the lower presence of metal oxides. Addition of CA has reduced the content of Ca and other metal ions in the nutrient-leached acid thus resulting in CA-hydrochar showing less ash content (65 %). High concentrations of P and Mg contributed to high ash content in the hydrochar and struvites. Similar observations on the high ash content of hydrochar, due to the high content of P and Ca were reported in previous studies on hydrochar [28,56].

3.7. Applicability of hydrochar and struvites as fertilizer

Middelton-Smith et al. compared different disposal pathways of hydrochar such as direct disposal, landfill, full valorization, combustion, struvite extraction, disposal after partial valorization, fertilizer and soil amendments etc. to reduce the liability to the commercialization of hydrochar [17]. As per U.S. Environmental Protection Agency (EPA) disposal regulations [57] hydrochar having solid ash content > 56 % and negligible hazardous characteristics associated with ignitability,

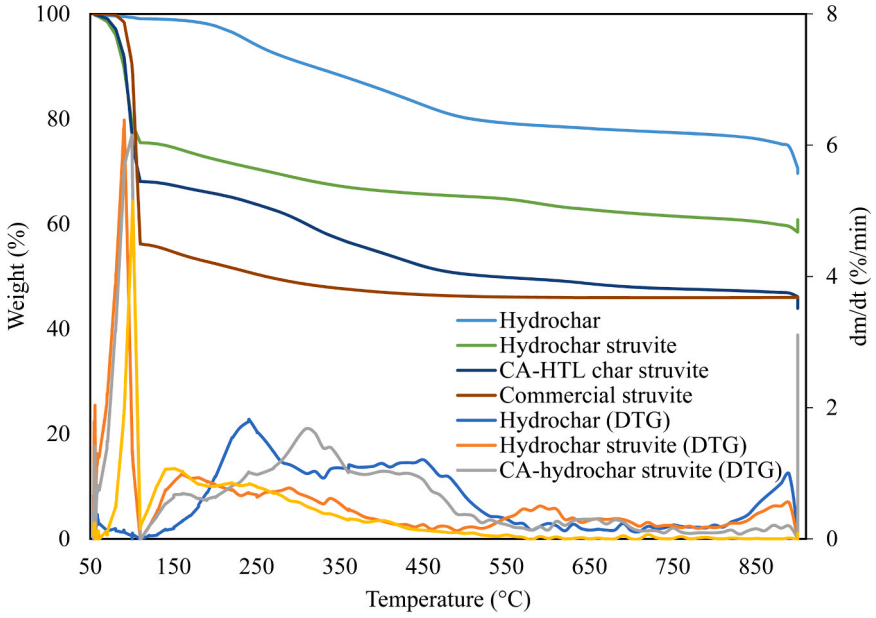

Fig. 5. TGA-DTG of hydrochar and struvites.

corrosivity, reactivity and toxicity (due to the high inorganic matter concentration) could be disposed of in landfills. However, recovery of nutrients was recommended as the presence of inorganic plant nutrients in hydrochar could allow its blending with existing fertilizer. According to the Danish decree on the use of waste for agricultural purposes [58], hydrochar was found unacceptable as it contained Ni (4745 mg/kg of P) more than the permissible limit (2500 mg/kg of P). It should be noted that the Ni content is suspected to originate from corrosion inside the hot solid separation unit, as the equivalent experiment in a batch reactor resulted in Ni content of 53 mg/kg from the identical feedstock [7]. Upon evaluation of hydrochar for agricultural purposes against the EU's fertilizer regulation (2019/1009), elevated content of Zn, Cu and Ni makes hydrochar unsuitable for direct application on agricultural land (Table 4). Nevertheless, the results are in overall accordance with heavy metal concentrations presented by PNNL on a variety of feedstocks that would also surpass the EU fertilizer limits including Ni, Zn and Cr [20]. Hydrochar struvite showed a reduction in Zn, Cu, Cr and Ni by 22 %, 70 %, 74 % and 94 %, respectively and helps to provide a promising perspective for land application as the Danish regulation, EPA and EU limits are thereby met. CA-hydrochar struvite further decreased the heavy metals content (240 mg/kg of Zn, 40 mg/kg of Cu, 15 mg/kg of Ni and ~7 mg/kg of Cr) which falls well within the permissible limits. Thus, CA-hydrochar struvite can be considered a cleaner fertilizer that covers the nutrient demand of crops and contributes less to heavy metal input to farmland than hydrochar and hydrochar struvite. The drawback being a lower total P recovery when the additional purity is obtained by addition of CA. Although the necessary fertilization regulations are more permissive and recovered struvite exhibits quality comparable to commercially available struvite, it is crucial to understand the effects of CA-hydrochar struvite in soil, crops, and P-bioavailability. Thus, encouraging the present results, further research is necessary to identify the influence of CA-hydrochar struvite on agricultural soil as well as crop growth. It is proposed to analyze the viability of process in terms of chemical ($MgCl_2$ and NaOH) consumption to analyze the economic balance of the process. Also, the possible pilot plant application of low-cost and eco-friendly P-loaded CA-hydrochar struvite should be investigated.

4. Conclusions

The present study explored a series of acid extractions to recover P from HTL of sewage sludge hydrochar, which leads a step towards sustainable management and conservation of resources. The overall findings of this investigation confirmed high P content (61,750 mg/kg) in hydrochar, low toxicity, PAH and PFAS content but elevated heavy metal content. Comparing extractions using different acids, sulfuric acid provided the highest P extraction (94 %) at the optimum condition of 0.7 mol/L acid strength and 6.5 h of leaching time. The highest P extraction with H_2SO_4 was due to the availability of double concentration of H^+ ions and by dissolving alkali-metal oxides and leaching P from organic and inorganic phases. The RSM models effectively established second-order polynomial model equation for each acid. Moreover, leached P was recovered in the form of an artificial fertilizer called hydrochar struvite. Compared to hydrochar, hydrochar struvite showed reduced heavy metals content (Zn, Cu, Ni and Cr by 22 %, 70 %, 94 % and 73 %, respectively). While the addition of CA during the struvite precipitation exhibited a significant reduction in Ca and heavy metals and an improvement in morphological properties. Total P recovery from the hydrochar to struvite was lower than in the literature with a maximum of 67 % which fell to 40 % with the addition of citric acid. Further optimization of the struvite precipitation step is suggested while the use of citric acid is shown to benefit the quality of struvite but will ultimately exhibit a trade of between heavy metal content and total P recovery.

CRediT authorship contribution statement

Shukla Neha: Writing – original draft, Visualization, Methodology, Investigation, Formal analysis, Data curation. **Leendert Vergeynst:** Writing – review & editing, Methodology, Investigation, Formal analysis. **Patrick Biller:** Writing – review & editing, Supervision, Project administration, Funding acquisition, Conceptualization.

Declaration of Competing Interest

The authors declare that they have no known competing financial interests or personal relationships that could have appeared to influence the work reported in this paper.

Data availability

Data will be made available on request.

Acknowledgement

This research was funded by the European Research Council (ERC) under the European Union's Horizon 2020 Research and Innovation Program grant No.849841 (REBOOT-Resource efficient bio-chemical production and waste treatment) and Det Energiteknologiske Udviklings- og Demonstrations Program (EUDP) Fund Denmark Nr. 64021-1076 (Sludge2Fuel).

Declaration of Competing Interest

The authors declare no known competing interests.

Appendix A. Supporting information

Supplementary data associated with this article can be found in the online version at doi:10.1016/j.jece.2024.113014.

References

[1] X. Wang, V. Wei-Chung Chang, Z. Li, Y. Song, C. Li, Y. Wang, Co-pyrolysis of sewage sludge and food waste digestate to synergistically improve biochar characteristics and heavy metals immobilization, Waste Manag. 141 (2022) 231–239, https://doi.org/10.1016/j.wasman.2022.02.001.
[2] S. Adhikari, H. Nam, J.P. Chakraborty, Conversion of solid wastes to fuels and chemicals through pyrolysis, Waste Biorefinery Potential Perspect. (2018) 239–263, https://doi.org/10.1016/B978-0-444-63992-9.00008-2.
[3] G.K. Gaurav, T. Mehmood, M. Kumar, L. Cheng, K. Sathishkumar, A. Kumar, D. Yadav, Review on polycyclic aromatic hydrocarbons (PAHs) migration from wastewater, J. Contam. Hydrol. 236 (2021) 103715, https://doi.org/10.1016/j.jconhyd.2020.103715.
[4] F. Fredriksson, U. Eriksson, A. Kärrman, L.W.Y. Yeung, Per- and polyfluoroalkyl substances (PFAS) in sludge from wastewater treatment plants in Sweden — first findings of novel fluorinated copolymers in Europe including temporal analysis, Sci. Total Environ. 846 (2022), https://doi.org/10.1016/j.scitotenv.2022.157406.
[5] Sludge EurEau, and the circular economy – the impact of PFAS, Brief, Note 6 (2022) 128.
[6] N. Gandhi, N. Farfaras, N.H.L. Wang, W.T. Chen, Life cycle assessment of recycling high-density polyethylene plastic waste, J. Renew. Mater. 9 (2021) 1463–1483, https://doi.org/10.32604/jrm.2021.015529.
[7] L.B. Silva Thomsen, K. Anastasakis, P. Biller, Hydrothermal liquefaction potential of wastewater treatment sludges: effect of wastewater treatment plant and sludge nature on products distribution, Fuel 355 (2024), https://doi.org/10.1016/j.fuel.2023.129525.
[8] F. Gievers, A. Loewen, M. Nelles, Life cycle assessment of sewage sludge pyrolysis: environmental impacts of biochar as carbon sequestrator and nutrient recycler, Detritus 16 (2021) 94–105, https://doi.org/10.31025/2611-4135/2021.15111.
[9] J. Havukainen, A. Saud, T.F. Astrup, P. Peltola, M. Horttanainen, Environmental performance of dewatered sewage sludge digestate utilization based on life cycle assessment, Waste Manag 137 (2022) 210–221, https://doi.org/10.1016/j.wasman.2021.11.005.
[10] C. Huang, B.A. Mohamed, L.Y. Li, Comparative life-cycle assessment of pyrolysis processes for producing bio-oil, biochar, and activated carbon from sewage sludge, Resour. Conserv. Recycl. 181 (2022) 106273, https://doi.org/10.1016/j.resconrec.2022.106273.

[11] X. Zhou, J. Li, X. Zhao, J. Yang, H. Sun, S.S. Yang, S. Bai, Resource recovery in life cycle assessment of sludge treatment: Contribution, sensitivity, and uncertainty, Sci. Total Environ. 806 (2022) 150409, https://doi.org/10.1016/j.scitotenv.2021.150409.
[12] L. Li, G. Du, B. Yan, Y. Wang, Y. Zhao, J. Su, H. Li, Y. Du, Y. Sun, G. Chen, W. Li, T. H. Pedersen, Carbon footprint analysis of sewage sludge thermochemical conversion technologies, Sustainability (2023).
[13] X.Y. Duan, Y. Cao, T.Z. Liu, L. Li, B. Wang, X.D. Wang, Nutrient stability and sorption of sewage sludge biochar prepared from co-pyrolysis of sewage sludge and stalks / mineral materials, Environ. Pollut. Bioavailab. 32 (2020) 12–18, https://doi.org/10.1080/26395940.2019.1710259.
[14] S. Neha, N. Remya, Raw and processed data set for optimization of bio-oil production from microwave co-pyrolysis of food waste and low-density polyethylene with response surface methodology, Data Br. 42 (2022) 108093, https://doi.org/10.1016/j.dib.2022.108093.
[15] H. Liu, I. Alper, A. Nzihou, C. Eskicioglu, Hydrochar derived from municipal sludge through hydrothermal processing: a critical review on its formation, characterization, and valorization, Water Res. 199 (2021) 117186, https://doi.org/10.1016/j.watres.2021.117186.
[16] A. Tripathi, N. Shukla, N. RemyaEffect of microwave susceptors on the microwave CO-pyrolysis of food waste and plastic.2019, , 1–2..
[17] L.A. Middleton-smith, A.H. Zacher, S. Blackwell, J. Benemann, T. Lundquist, Disposition of solids from hydrothermal liquefaction of biomass: current understanding, Res. Gaps Oppor. (2023), https://doi.org/10.1021/acs.energyfuels.3c01828.
[18] A. Matayeva, S.R. Rasmussen, P. Biller, Biomass and Bioenergy Distribution of nutrients and phosphorus recovery in hydrothermal liquefaction of waste streams, Biomass Bioenergy 156 (2022) 106323, https://doi.org/10.1016/j.biombioe.2021.106323.
[19] E. Ovsyannikova, A. Kruse, G.C. Becker, Valorization of byproducts from hydrothermal liquefaction of sewage sludge and manure: the development of a struvite-producing unit for nutrient recovery, Energy Fuels 35 (2021) 9408–9423, https://doi.org/10.1021/acs.energyfuels.1c00561.
[20] H. Liu, G. Hu, I. Alper, J. Li, N. Lyczko, A. Nzihou, C. Eskicioglu, Phosphorus recovery from municipal sludge-derived ash and hydrochar through wet-chemical technology: a review towards sustainable waste management, Chem. Eng. J. 417 (2021) 129300, https://doi.org/10.1016/j.cej.2021.129300.
[21] R. Ravi, M. Beyers, S. Bruun, E. Meers, Resources, Conservation & Recycling Life cycle assessment of struvite recovery and wastewater sludge end-use: a Flemish illustration, Resour. Conserv. Recycl. 182 (2022) 106325, https://doi.org/10.1016/j.resconrec.2022.106325.
[22] M.M. Kasina, K. Joseph, M. John, Application of central composite design to optimize spawns propagation, Open J. Optim. (2020) 47–70, https://doi.org/10.4236/ojop.2020.93005.
[23] H. Xu, P. He, W. Gu, G. Wang, L. Shao, Recovery of phosphorus as struvite from sewage sludge ash, J. Environ. Sci. 24 (2012) 1533–1538, https://doi.org/10.1016/S1001-0742(11)60969-8.
[24] L. Sun, Y. Yang, W. Yuan, X. Wu, Z. Cui, H. Wang, H. Deng, X. Zhu, R. Li, Struvite purity prediction by response surface methodology and chemical equilibrium modeling combination, Environ. Technol. Innov. 29 (2023) 103016, https://doi.org/10.1016/j.eti.2023.103016.
[25] L. Bjørn, S. Thomsen, P.N. Carvalho, J. Souza, K. Anastasakis, K. Bester, P. Biller, Hydrothermal liquefaction of sewage sludge; energy considerations and fate of micropollutants during pilot scale processing, Water Res 183 (2020) 116101, https://doi.org/10.1016/j.watres.2020.116101.
[26] International Standard Method 11348-3, Water quality — Kinetic determination of the inhibitory effects of sediment, other solids and coloured samples on the light emission of Vibrio fischeri (kinetic luminescent bacteria test), (2010).
[27] M.J. Rivas-arrieta, C. Torri, A.G. Rombol, P. Biller, Hydrochar fractionation Compos. batch Contin. hydrothermal Liq. Biomass Bioenergy 183 (2024) https://doi.org/10.1016/j.biombioe.2024.107166.
[28] M. Xu, Y. Wang, T. Liu, L. Yang, H. Liu, D. Xu, Biomass and Bioenergy Evaluation on phosphorus extraction potential in hydrochar obtained from hydrothermal liquefaction of sewage sludge, Biomass Bioenergy 182 (2024) 107121, https://doi.org/10.1016/j.biombioe.2024.107121.
[29] H. Liu, G. Hu, I.A. Basar, J. Li, N. Lyczko, A. Nzihou, C. Eskicioglu, Phosphorus recovery from municipal sludge-derived ash and hydrochar through wet-chemical technology: a review towards sustainable waste management, Chem. Eng. J. 417 (2021), https://doi.org/10.1016/j.cej.2021.129300.
[30] K. Hong, N. Tarutani, Y. Shinya, T. Kajiuchi, K. Hong, N. Tarutani, Y. Shinya, Study on the recovery of phosphorus from waste- activated sludge incinerator ash study on the recovery of phosphorus from waste-activated sludge incinerator ash, J. Environ. Sci. Health A Tox. Hazard. Subst. Environ. Eng. 4529 (2007), https://doi.org/10.1081/ESE-200046614.
[31] S. Liang, H. Chen, X. Zeng, Z. Li, W. Yu, K. Xiao, J. Hu, H. Hou, B. Liu, S. Tao, J. Yang, A comparison between sulfuric acid and oxalic acid leaching with subsequent purification and precipitation for phosphorus recovery from sewage sludge incineration ash, Water Res. 159 (2019) 242–251, https://doi.org/10.1016/j.watres.2019.05.022.
[32] Q. Chen, J. Qin, P. Sun, Z. Cheng, G. Shen, Cow dung-derived engineered biochar for reclaiming phosphate from aqueous solution and its validation as slow-release fertilizer in soil-crop system, J. Clean. Prod. (2018), https://doi.org/10.1016/j.jclepro.2017.11.224.
[33] M. Fernández-delgado, E. Amo-mateos, M.T. García-cubero, S. Lucas, Phosphorus recovery from organic waste for its agronomic valorization, Tech. Econ. Eval. (2021), https://doi.org/10.1002/jctb.6926.
[34] E. Karabacak, Phosphorus Recovery by Chemical Extraction from Different Types of Air Pollution Control Ashes of Sludge Incinerators, (2022).
[35] H. Elomaa, S. Seisko, J. Lehtola, M. Lundström, A study on selective leaching of heavy metals vs. iron from fly ash, J. Mater. Cycles Waste Manag. 21 (2019) 1004–1013, https://doi.org/10.1007/s10163-019-00858-w.
[36] G. Jabr, M. Saidan, N. Al-Hmoud, Phosphorus recovery by struvite formation from al samra municipal wastewater treatment plant in jordan, Desalin. Water Treat. 146 (2019) 315–325, https://doi.org/10.5004/dwt.2019.23608.
[37] S. Polat, H. Burak, Effect of hyaluronic acid on the struvite crystallization: a structural, morphological, and thermal analysis study, J. Cryst. Growth 592 (2022) 126734, https://doi.org/10.1016/j.jcrysgro.2022.126734.
[38] X. Lu, W. Xu, Q. Zeng, W. Liu, F. Wang, Quantitative, morphological, and structural analysis of Ni incorporated with struvite during precipitation, Sci. Total Environ. 817 (2022) 152976, https://doi.org/10.1016/j.scitotenv.2022.152976.
[39] L. Bianchi, K. Kirwan, L. Alibardi, M. Pidou, S.R. Coles, Recovery of ammonia from wastewater through chemical precipitation: Investigating the kinetic mechanism and reactions pathway of struvite decomposition, J. Therm. Anal. Calorim. 142 (2020) 1303–1314, https://doi.org/10.1007/s10973-019-09108-5.
[40] Y. Song, Y. Dai, Q. Hu, X. Yu, F. Qian, Effects of three kinds of organic acids on phosphorus recovery by magnesium ammonium phosphate (MAP) crystallization from synthetic swine wastewater, Chemosphere 101 (2014) 41–48, https://doi.org/10.1016/j.chemosphere.2013.11.019.
[41] W. Wang, X. Xin, B. Li, H. Huang, X. Liu, L. Song, X. Wu, Y. Huang, Effect of organics on Cu and Cr in recovered struvite from synthetic swine wastewater, J. Clean. Prod. 360 (2022) 132186, https://doi.org/10.1016/j.jclepro.2022.132186.
[42] I.D.A.A. Warmadewanthi, M.A. Zulkarnain, N. Ikhlas, S.B. Kurniawan, S.R. S. Abdullah, Struvite precipitation as pretreatment method of mature landfill leachate, Bioresour. Technol. Rep. 15 (2021) 100792, https://doi.org/10.1016/j.biteb.2021.100792.
[43] S. Wang, K. Sun, H. Xiang, Z. Zhao, Y. Shi, L. Su, C. Tan, L. Zhang, Biochar-seeded struvite precipitation for simultaneous nutrient recovery and chemical oxygen demand removal in leachate: from laboratory to pilot scale, Front. Chem. 10 (2022) 1–14, https://doi.org/10.3389/fchem.2022.990321.
[44] A. Siciliano, Assessment of fertilizer potential of the struvite produced from the treatment of methanogenic landfill leachate using low-cost reagents, Environ. Sci. Pollut. Res. 23 (2016) 5949–5959, https://doi.org/10.1007/s11356-015-5846-z.
[45] G.C. Becker, D. Wüst, H. Köhler, A. Lautenbach, A. Kruse, Novel approach of phosphate-reclamation as struvite from sewage sludge by utilising hydrothermal carbonization, J. Environ. Manag. 238 (2019) 119–125, https://doi.org/10.1016/j.jenvman.2019.02.121.
[46] C. Numviyimana, J. Warcho, N. Khalaf, J.J. Leahy, Phosphorus recovery as struvite from hydrothermal carbonization liquor of chemically produced dairy sludge by extraction and precipitation, J. Environ. Chem. Eng. 10 (2022), https://doi.org/10.1016/j.jece.2021.106947.
[47] A. Gianico, C.M. Braguglia, A. Gallipoli, D. Montecchio, G. Mininni, Land application of biosolids in europe: possibilities, con-straints and future perspectives, Water (Switz.) 13 (2021), https://doi.org/10.3390/w13010103.
[48] H. Yan, K. Shih, Effects of calcium and ferric ions on struvite precipitation: a new assessment based on quantitative X-ray diffraction analysis, Water Res. 95 (2016) 310–318, https://doi.org/10.1016/j.watres.2016.03.032.
[49] X. Liu, J. Wang, Impact of calcium on struvite crystallization in the wastewater and its competition with magnesium, Chem. Eng. J. 378 (2019) 122121, https://doi.org/10.1016/j.cej.2019.122121.
[50] J. Hövelmann, T.M. Stawski, R. Besselink, H.M. Freeman, K.M. Dietmann, S. Mayanna, B.R. Pauw, L.G. Benning, A template-free and low temperature method for the synthesis of mesoporous magnesium phosphate with uniform pore structure and high surface area, Nanoscale 11 (2019) 6939–6951, https://doi.org/10.1039/c8nr09205b.
[51] D. Sidorczuk, M. Kozanecki, B. Civalleri, K. Pernal, J. Prywer, Structural and optical properties of struvite. Elucidating structure of infrared spectrum in high frequency range, J. Phys. Chem. A 124 (2020) 8668–8678, https://doi.org/10.1021/acs.jpca.0c04707.
[52] L.B. Moyo, G.S. Simate, N. Hobane, C. Dube, Characterization, kinetics and thermodynamic evaluation of struvite produced using ferrochrome slag as a magnesium source, S. Afr. J. Chem. Eng. 47 (2024) 83–90, https://doi.org/10.1016/j.sajce.2023.10.012.
[53] B. Tansel, G. Lunn, O. Monje, Struvite formation and decomposition characteristics for ammonia and phosphorus recovery: A review of magnesium-ammonia-phosphate interactions, Chemosphere 194 (2018) 504–514, https://doi.org/10.1016/j.chemosphere.2017.12.004.
[54] J. Hövelmann, T.M. Stawski, R. Besselink, H.M. Freeman, K.M. Dietmann, S. Mayanna, B.R. Pauw, L.G. Benning, A template-free and low temperature method for the synthesis of mesoporous magnesium phosphate with uniform pore structure and high surface area, Nanoscale 11 (2019) 6939–6951, https://doi.org/10.1039/c8nr09205b.
[55] R. Yu, H. Ren, Y. Wang, L. Ding, J. Geng, K. Xu, Y. Zhang, A kinetic study of struvite precipitation recycling technology with NaOH/Mg(OH)2 addition, Bioresour. Technol. 143 (2013) 519–524, https://doi.org/10.1016/j.biortech.2013.06.042.

[56] T. Wang, M. Camps-Arbestain, M. Hedley, B.P. Singh, R. Calvelo-Pereira, C. Wang, Determination of carbonate-C in biochars, Soil Res. 52 (2014) 495–504, https://doi.org/10.1071/SR13177.

[57] ⟨https://www.ecfr.gov/current/title-40/chapter-I/subchapter-O/part-503/subpart-B/section-503.13⟩, eCFR _ 40 CFR 503, (n.d.).

[58] Danish Ministry of Environment, Bekendtgørelse om anvendelse af affald til jordbrugsformål, Retsinformation 2018 (2018) 1–18.